Analytical Study on the Elastic-Plastic Transition in Short Fiber Reinforced Composites

Hong Gun Kim*

(*Received July 30, 1997*)

In discontinuous composites, the fiber end effects can be neglected when the length of fiber is much greater compared to the diameter. Thus, conventional shear lag theory is very useful for predicting composite properties deduced from each constituent. However, in the case of short fiber or whisker reinforced composites, the end effects cannot be neglected, and the composite properties are functions of material and geometrical parameters since the fiber end effects significantly influence the behavior of composites. For a good understanding of the behavior of short fiber or whisker reinforced composites, it is necessary to first understand the mechanism of stress transfer and it has well been modified before. However, the modification was limited to the basic elastic stress calculation of the fiber and matrix in a micromechanical model. Accordingly, the former modification of the shear lag model has been extended to predict the overall elastic composite behavior and elastic-plastic behavior of which result can predict the stress concentration in the matrix as well as the onset of matrix yielding. The extended modification results showed that it gives a good agreement with finite element analysis as well as with experimental data. It was also found that the local matrix yielding is initiated in the vicinity of the fiber ends which produces local plasticity and an elastic-plastic transition before the composite stress reaches matrix yield stress.

Key Words: Shear Lag Theory, Discontinuous Composite, Fiber Aspect Ratio, Elastic Behavior, Stress Concentration, FEA, Matrix Yielding

1. Introduction

Composites, man-made material in which two or more constituents are combined to create a material with properties different from that of either constituent, have been excited for thousands of years (Nair et al., 1985). The objective of fabricating composites is to improve mechanical properties such as strength, stiffness, toughness and high temperature performance. Therefore, it is natural to study composites that have a common strengthening mechanism.

In these composites, loads are not directly applied to the fibers but are applied to the matrix material and transferred to the fibers through the fiber ends and also through the cylindrical surface of the fiber near ends (Piggot, 1980). The stress transfer is mainly due to the shearing mechanism through the cylindrical surface of the fiber near ends if the fiber aspect ratio is not small, which induces the conventional shear lag (SL) theory (Cox, 1952). The SL model, which considers long straight discontinuous fibers completely embedded in a continuous matrix, is originated from Cox.

However, a major shortcoming of the Cox model is in its inability to provide sufficiently accurate predictions when the fiber aspect ratio is small. The predicted modulus by the SL model is substantially smaller than the experimentally observed modulus increase in this regime. This is the regime applicable to major current short fiber or whisker reinforced composites. For example, in SiC whisker reinforced Al alloys, the average

* Department of Mechanical Engineering, Jeonju University, 1200 Hyojadong 3 Ga, Wansangu, Jeonju 560-759, Korea.

aspect ratio is only on the order of four (Arsenault, 1984, Nair et al., 1985, Nutt and Needleman, 1987), and for this case the original SL model does not provide an adequate description of the stiffening effect of fibers or whiskers as discussed by Taya and Arsenault (1987).

Following the the Cox model, rigorous elasticity models based on a variational approach (Hashin and Shtrikman, 1962, 1963) and self-consistent method (Hill, 1965a) were developed in order to predict the elastic moduli increases in the small aspect ratio regime. The variational method originally developed by Paul (1960) provides proper bounds to the elastic moduli increases but not to the local stress values in the fiber and surrounding matrix. In fact, the self-consistent model was first developed by Hershey (1954) and Kroner (1958) as a means to model the behavior of polycrystalline materials, and an extension of the self-consistent scheme to multiphase media was given by Hill (1965b) and Budiansky (1965). This method provides an approximate prediction of composite elastic response that explicitly accounts for phase geometry. Eshelby's ellipsoidal inclusion method (Eshelby, 1957) is a basic solution of this type and has also been successfully applied to predict both the modulus and yield strength of short fiber composites (Taya and Arsenault, 1987).

However, this model is restricted to ellipsoidal reinforcement geometries in which the internal reinforcement stress is assumed to be uniform. It is well known that for the case of rod-like fiber geometries, uniform reinforcement stresses are obtained only at sufficiently large aspect ratios. Furthermore, the shear stress transfer gives rise to known variations of the fiber axial stresses (Piggot, 1980). Accordingly, the SL approach is physically more realistic for fiber geometries provided that fiber end effects can be rigorously accounted for.

There have been limited previous attempts to modify the SL approach. Muki and Sternberg (1969) and Sternberg and Muki (1970) used the SL approach in a more refined manner using *integro-differential equations* and have calculated the local stresses inside the fiber. However, this model assumed that the fiber center stress is given by the rule of mixture equation strictly applicable only to the long fiber case. Furthermore, Sternberg's results cannot be applied to obtain expressions for the matrix stress intensification in the fiber end region which provides a significant contribution to the elastic modulus (Halpin, 1984 and Hashin, 1983).

Nardone and Prewo (1986) and Nardone (1987) attempted to modify the SL model by assuming that the fiber end stress, was equal to the matrix yield stress and that the matrix average stress was also equal to the matrix yield stress.

The calculation using this model showed quite crude results in Al/SiC composites (Taya and Arsenault, 1987).

Taya and Arsenault (1989) also attempted to modify the original SL approach by assuming that the fiber end stress was equal to the average matrix stress, i. e., the stress concentration at the fiber ends were ignored. The prediction of this limited modification is compared to that of the rigorous model presented below.

Recently, Kim and Nair (1990) also modified the SL analysis by using FEA to provide the fiber end normal stresses. While their work clearly demonstrates that SL solutions are applicabe to short fiber composites provided fiber end effects are accounted for, the model does not calculate the fiber end stresses from first principles and relies instead on FEA.

More recently, Kim (1994) derived the modified shear lag (MSL) theory showing elastic stress transfer mechanism using fictitious fiber concept. The approach in his work involved replacing the matrix region between fiber ends with a fictitious fiber having the same elastic properties as the matrix and developing conventional SL solutions for both the *real and fictitious* fiber. Suitable interfacing of these solutions provides the needed results for the local stress and strain values. The model is therefore entirely closed form in nature and does not rely on FEA for any parametric values.

The purpose of this study is to extend a straightforward yet rigorous derivation of the MSL analysis to predict the overall elastic behav-

ior and the elastic-plastic transition so as to monitor the onset of matrix yielding. It was attempted to retain accuracy at both small and large fiber aspect ratio values by taking fiber end effects into account even in the elastic-plastic transient state. An axisymmetric FEA model along with experimental data have been implemented to evaluate the predictions of the analytical model derived in this paper.

2. Analytical Approach

The conventional SL model is based on the concept that fiber tensile stresses are governed by an interfacial shear stress parallel to the fiber surface. The theory is described in the paper of Kim (Kim, 1994). A micromechanical model deduced from physical concepts is described as follows. The discontinuous short fibers or whiskers are considered to be uniaxially aligned with the stress applied in the axial direction of the fibers. The fiber/matrix bond is assumed to be large, and no debonding is allowed in keeping with the actual situation in many MMCs (Arsenault, 1983). Further, no plastic yielding is allowed; that is, both matrix and fiber deform in a purely elastic manner. The composite unit cell or representative volume element (RVE) showing the short fiber embedded in a continuous matrix is shown in Fig. 1.

As can be seen in the figure, the RVE has length $2L$, diameter D, fiber length $2l$, and fiber diameter d. Hereafter, the axial direction is expressed as x instead of z for convenience. The rationale for the modification is an attempt to understand the elastic behavior of composites taking fiber end stress transfer into account as shown in Fig. 2.

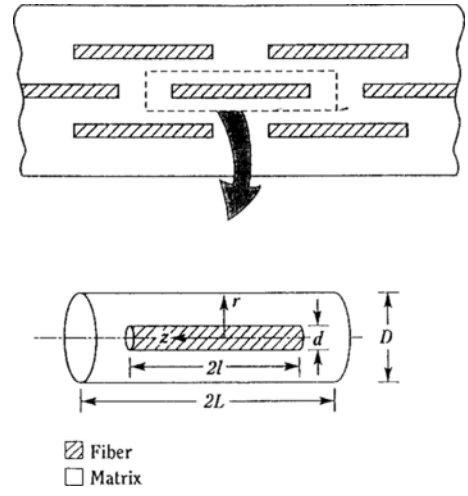

Fig. 1 Composite RVE containing a single fiber or whisker in a cylindrical matrix volume.

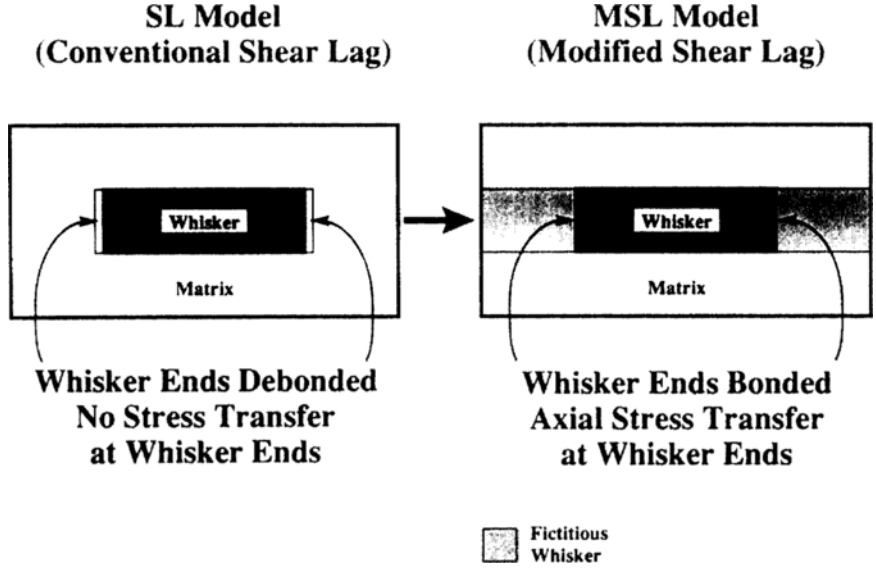

Fig. 2 Concept of the modification process introducing fictitious fiber or whisker.

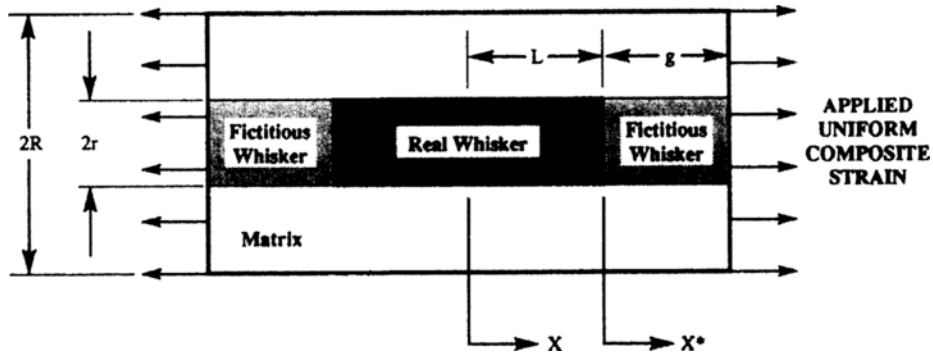

Fig. 3 The RVE of MSL model. Matrix end gap regions are replaced by fictitious fiber or whisker to maintain the displacement and traction compatibility in the MSL model.

The modified composite unit cell (RVE) showing the short fiber embedded in a continuous matrix is shown in Fig. 3. The actual, or real, fiber has radius and length $2L$. On either end of the fiber we assume a fictitious fiber of diameter $2r$ and length g equal to half the spacing between the fiber ends in the composite. The outer surface of the unit cell can be said to have a hexagonal contour, although, the exact shape is not critical in this model. The unit cell is treated as an equivalent cylinder with radius R. The spatial variable for the real fiber is x, with the coordinate origin at the fiber center, whereas the spatial variable for the fictitious fiber is x^* with the coordinate origin at the fiber end. The different origins are necessary because, as will be shown, the governing differential equations in the region of the real and fictitious fiber are different and consequently there can be no overlap of the x and x^* domains. The two domains are in contact at $x=L$, or $x^*=0$, at which point proper boundary conditions need to be applied. Note in the following that all variables associated with the fictitious fiber will be denoted with a superscript $*$. At the far end of the unit cell, that is, at the surface $x^*=g$, a uniform constant composite strain ε_c is applied. Under these conditions, as shown in detail in the SL model (Piggot, 1980), the governing equation for the fiber stress, σ_f, and the fiber/matrix interfacial shear stress, τ_s, can be given by the same type. (Kim, 1994).

As derived from the previous study (Kim, 1994), the combination of equilibrium conditions and Hook's Law gives a governing differential equation for the real fiber or whisker as below:

$$\frac{d^2\sigma_f}{dx^2}=\frac{n^2}{r^2}(\sigma_f-E_f\varepsilon_c) \tag{1}$$

where

$$n^2=\frac{E_m}{E_f(1+\nu_m)\ln(R/r)} \tag{2}$$

Here E_m and E_f are Young's moduli of the matrix and fiber, respectively, V_f is the volume fraction of fiber and ν_m is Poisson's ratio for the matrix. As mentioned above, R is the unit cell radius. Hence, the governing differential equation for the fictitious fiber or whisker is given by

$$\frac{d^2\sigma_f^*}{dx^{*2}}=\frac{n^{*2}}{r^2}(\sigma_f^*-E_f\varepsilon_c^*) \tag{3}$$

Since $E_f=E_m$ one obtains

$$n^{*2}=\frac{1}{(1+\nu_m)\ln(R/r)} \tag{4}$$

Equations (1) and (3) admit the solution as shown below. Detailed procedures of the derivation can be found in the previous paper (Kim, 1994).

$$\sigma_f=E_f\varepsilon_c+A\sinh(nx/r)+B\cosh(nx/r) \tag{5}$$

$$\sigma_f^*=E_m\varepsilon_c+A^*\sinh(n^*x^*/r)+B^*\cosh(n^*x^*/r) \tag{6}$$

$$\tau_s=-\frac{n}{2}B\sinh(nx/r) \tag{7}$$

$$\tau_s^*=-\frac{n^*}{2}[A^*\cosh(n^*x^*/r)$$

$$+B^*\sinh(n^*x^*/r)] \tag{8}$$

Here, $A^*\neq 0$ since the end regions do not possess the symmetry of the fiber because of the coordinate change. Therefore, the three unknown constants in Eq. (5) to (8) are B, A^* and B^*, which can be simply determined using the following boundary conditions. To satisfy displacement and traction compatibility:

$$\sigma_f=\sigma_f^* \text{ at } x=L \text{ or } x^*=0 \tag{9}$$

$$\frac{d\sigma_f}{dx}=\frac{d\sigma_f^*}{dx^*} \text{ at } x=L \text{ or } x^*=0 \tag{10}$$

$$\tau_s^*=0 \text{ at } x^*=g \tag{11}$$

The first condition sets the fiber/matrix interfacial normal stress at the fiber end to be the same in both regions. The second requires that the shear stress at the fiber/matrix interface also be the same in the limit $x\rightarrow L$ and $x^*\rightarrow 0$. These are necessary continuity conditions. The final condition is based on the iso-strain condition of the problem, namely, that the applied strain is uniform across the transverse boundary of the RVE at $x^*=g$. This requires that the shear stress be also zero at $x^*=g$. It can then be shown that the unknown constants are given by:

$$A=0 \tag{12}$$

$$B=\frac{(E_m-E_f)\,\varepsilon_c}{\cosh(ns)+(n/n^*)\sinh(ns)\coth(n^*s^*)} \tag{13}$$

$$A^*=-B^*\tanh(n^*s^*) \tag{14}$$

$$B^*=-B(n/n^*)\sinh(ns)\coth(n^*s^*) \tag{15}$$

where $s(=L/r)$ is the fiber aspect ratio and s^* $(=g/r)$ is the aspect ratio of the fictitious fiber. Hence, the fiber maximum stress σ_{fm} can be obtained by setting $x=0$ in Eq. (5):

$$\sigma_{fm}=E_f\varepsilon_c+B \tag{16}$$

In the same manner, the fiber end stress σ_i can also be obtained by setting $x^*=0$ in Eq. (6), namely:

$$\sigma_i=E_m\varepsilon_c+B^* \tag{17}$$

Hence B^* can be expressed as a function of ε_c and the result is given by

$$\sigma_i=(E_m+C)\,\varepsilon_c \tag{18}$$

where

$$C=\frac{(E_m-E_f)\,(n/n^*)\sinh(ns)\coth(n^*s^*)}{\cosh(ns)+(n/n^*)\sinh(ns)\coth(n^*s^*)} \tag{19}$$

Therefore, Eq. (18) represents the interfacial stress between the real fiber and the fictitious fiber. As presumed, it is proportional to the composite strain. On this basis the stress concentration factor in the matrix K_t can be calculated in closed form as

$$\begin{aligned}K_t&=\frac{\sigma_i}{\bar{\sigma}_m}\\&=\frac{\sigma_i}{E_m\varepsilon_c}\\&=1+\frac{C}{E_m}\end{aligned} \tag{20}$$

Here, $\bar{\sigma}_m$ denotes the average stress of the matrix. It is important that the stress intensification in the fictitious fiber region is represented by Eq. (20). The composite stress can be determined from the rule of averages or the rule of mixture (ROM) as

$$\begin{aligned}\sigma_c&=V_f\bar{\sigma}_f+V_m\bar{\sigma}_m\\&=V_f\bar{\sigma}_f+V_f^*\bar{\sigma}_f^*+(V_m-V_f^*)\,\bar{\sigma}_m\end{aligned} \tag{21}$$

The dashed line above the variable indicates average values. These average values can be determined as follows:

$$\bar{\sigma}_f=\frac{1}{L}\int_0^L\sigma_f dx \tag{22}$$

$$\bar{\sigma}_f^*=\frac{1}{g}\int_L^{L+g}\sigma_f^* dx \tag{23}$$

$$\bar{\sigma}_m=E_m\varepsilon_c \tag{24}$$

The normalized longitudinal Young's modulus of the composite E_c/E_m can then be calculated. The final result for the modulus enhancement can then be given by Eq. (25) as below.

$$\begin{aligned}\frac{E_c}{E_m}=&\frac{E_fV_f}{E_m}+\frac{V_fB}{E_m\varepsilon_c}\sinh(ns)+V_m\\&+\frac{V_f^*}{E_m\varepsilon_c n^*s^*}[A^*(\cosh(n^*s^*)-1)\\&+B^*\sinh(n^*s^*)]\end{aligned} \tag{25}$$

It can be found that the above normalized modulus represents the composite strengthening effect which gives an elastic behavior. This phenomenon is shown in Fig. 4 which describes the

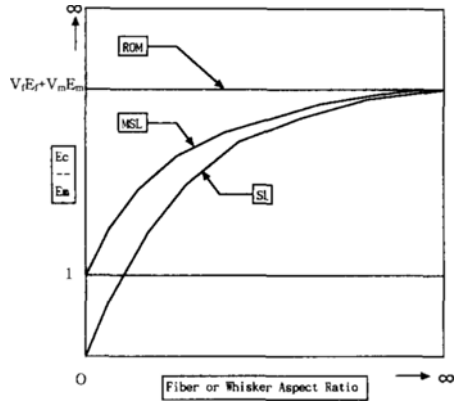

Fig. 4 Conceptual Schematic of ROM, SL, and MSL models.

concept of ROM, SL, and MSL models.

On the other hand, the matrix stress between fiber ends becomes greater and this stress will be reached at the yield point of the matrix. This localized matrix yielding is initiated in the vicinity of the fiber ends and occurs at the applied stress below matrix yield stress because of the stress concentration. Thus, the elastic proportional limit strain ε_{cp} will be reached when σ_i becomes the matrix yield stress σ_{my} as applied from Eq. (20). Therefore, this relation can be derived as follows.

$$\varepsilon_{cp}=\frac{\sigma_{my}}{(E_m+C)} \tag{26}$$

Thus, the elastic proportional limit of the composite stress, σ_{cp} is given by

$$\sigma_{cp}=E_c\varepsilon_{cp}=\frac{E_c}{(E_m+C)}\sigma_{my} \tag{27}$$

3. Finite Element Modeling for Verification

The application of FEA to composites requires careful attention to the geometry of the mesh used in analysis and design. In a discontinuous fiber reinforced composite, appropriate modeling is important in understanding the deformation evolution in the matrix as well as the overall composite stress-strain behavior except in very low fiber volume fraction cases (Agarwal *et al.*, 1974). The

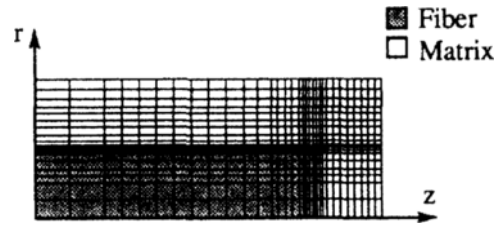

Fig. 5 Finite element mesh of the axisymmetric RVE ($V_f=20\%$).

2-D multiple fiber model used to develop the physical concepts was considered first for the aligned fiber geometry.

In this study, the FEA computations were performed using four-noded axisymmetric isoparametric elements (Cook et al., 1989) using the ANSYS program (Kohnke, 1989). Provided the fiber or whisker distribution is perfectly uniform, a single fiber model as RVE can be selected as mentioned above. The RVE selected along with the corresponding mesh patterns are shown in Fig. 5. The RVE is based on a finite concentration of 20% fibers which is quite common (see Fig. 5). The RVE configuration is similar to that used previously by Agarwal et al. (1974) and Kim and Chang (1995) for a uniform distribution of fiber with an end gap value equal to the transverse spacing between fibers. In other words, g is equal to $(R-r)$. This allows for comparison of volume fraction effects by both FEA and the analytical model developed in the previous section. For boundary conditions, constraint conditions were imposed by requiring that the longitudinal cell boundary (side wall) and the cell end should be undistorted during deformation as implemented in the previous work (Kim, 1990).

Material properties selected are Al 2124 as the matrix and SiC whisker as the reinforcement. For the present system, typical values are $E_m=67.2$ GPa, $\nu_m=0.33$ for the matrix and $E_f=480$ GPa, $\nu_f=0.17$ for the reinforcement (Nair et al., 1985).

4. Results and Discussion

In the previous paper (Kim, 1994), axial tensile stress, interfacial shear stress, and fiber maximum stress in the fiber and matrix end region (ficti-

tious fiber) have been described in detail. The present results of the extended MSL model are now shown in what follows.

4.1 Fiber end stress and stress concentration factor

As mentioned previously, the tensile stress in the matrix end region in the SL model is assumed constant throughout the gap region and equal to the average matrix stress ($=E_m\varepsilon_c$). In the MSL model, the fiber stresses are significantly higher than that in the SL model. These fiber stresses drop off to a finite interfacial value σ_i at the fiber end. For finite fiber concentrations ($V_f=20\%$),

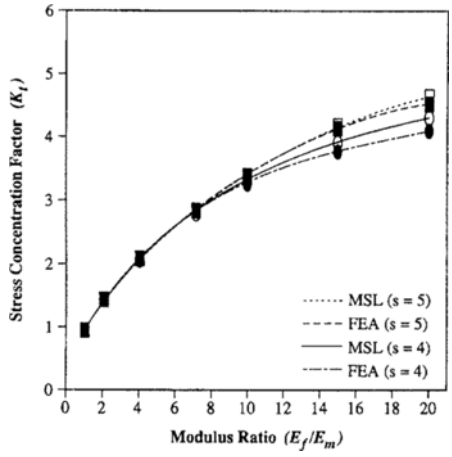

Fig. 6 Stress concentration factor as a function of modulus ratio at $\varepsilon_c=0.1\%$ in case of $V_f=20\%$.

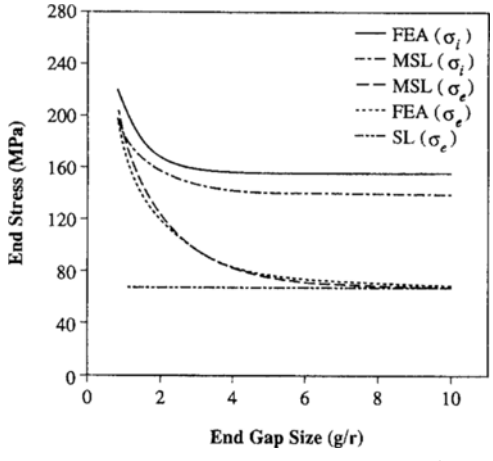

Fig. 7 End stress as a function of end gap size at $\varepsilon_c=0.1\%$ in case of $V_f=20\%$.

the results are shown in Figs. 6 and 7. Here, numerical values were set as $r=1$, $L=4$, $g=1$, $s=4$, $s^*=1$, $R/r=2$, $n=0.3897$ and $n^*=1.0415$.

The axial stresses at the fiber end derived in the MSL model (equation (18)), which represents the stress concentration factor K_t, are shown in Fig. 6 as a function of E_f/E_m for two fiber aspect ratio values in terms of the stress intensification $\sigma_i/E_m\varepsilon_c$, where $E_m\varepsilon_c$ is the average matrix stress. As shown in the Fig. 6, the results show remarkable agreement with the predicted FEA results.

There are two fiber end stresses: the real fiber end stress σ_i, and the fictitious fiber end stress σ_e. The real fiber end stresses σ_i, are also dependent on the end gap size (the length of fictitious fiber) as shown in Fig. 7. As the end gap size is reduced, the end stresses are significantly enhanced. These fiber end effects become more dominant for stiffer fibers, and for small fiber-to-fiber spacing in the end gap region. Note from the previous paper (Kim, 1994), that the matrix stresses in the end gap region are larger than the average matrix stress, predicted by the SL model. Thus, fiber end gap stresses and σ_i increase as the fibers come close together along the axial direction.

As shown in Fig. 7, σ_e is the fictitious fiber end stress (i. e., stress at $x=L+g$). Note that $\sigma_e \geq E_m\varepsilon_c$ because of the isostrain boundary condition, which means the fictitious fiber end stress must be equal to or greater than the matrix average stress $E_m\varepsilon_c$, since the fictitious fiber is, in reality, the region of stress concentration. The fictitious fiber end stress σ_e increases as the end gap size is reduced.

In comparison, as mentioned before, the SL model does not derive equations for the stresses in the matrix end gap (fictitious fiber) region. Consequently, it is found that $\sigma_e=E_m\varepsilon_c$ for the SL model case though it is the domain affected by stress concentration. When the matrix end gap size is increased indefinitely, σ_e from the MSL model approaches $E_m\varepsilon_c$ as expected.

4.2 Longitudinal composite Young's Modulus prediction and comparison with other theories and experimental data

The overall increase in composite modulus $E_c/$

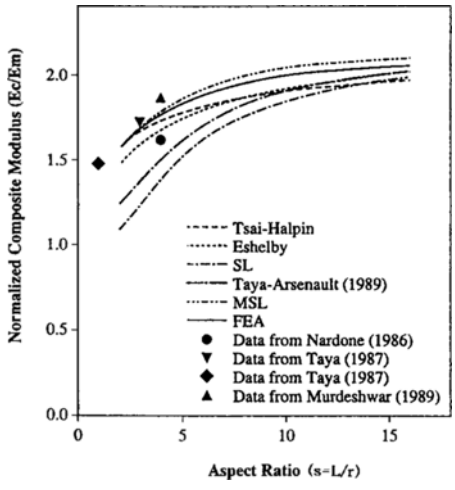

Fig. 8 Normalized composite longitudinal Young's modulus ratio as predicted by SL, MSL, and FEA as a function of aspect ratio ($s=L/r$) compared with other strengthening models ($E_f/E_m=7.14$). Filled symbols represent experimental data whereas each line indicates the theory prediction according to various models.

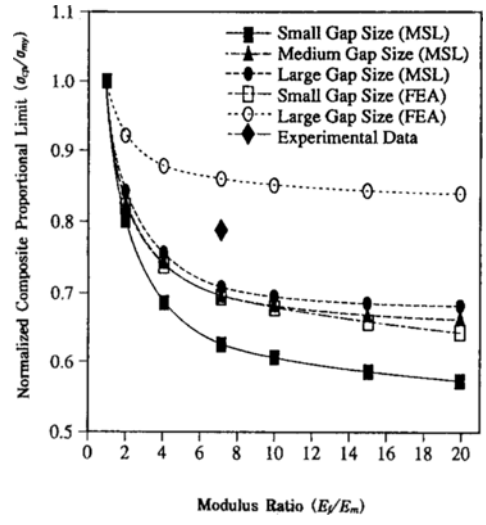

Fig. 9 The normalized composite proportional limit predicted by FEA and MSL based on small scale yielding as a function of the modulus ratio, E_f/E_m, for different gap sizes.

E_m (Eq. (25)) of the MSL model is plotted in Fig. 8 for two aspect ratio values as a function of E_f/E_m, the ratio of fiber to matrix modulus. Also shown for comparison is the corresponding FEA results. Again, there is a remarkable coincidence between the MSL and FEA results. The result of Fig. 8 shows without doubt that the shear lag approach suitably modified by taking the fiber end region stresses into account provides correct modulus prediction when the aspect ratio is small.

The dependence of E_c/E_m on the fiber aspect ratio for fixed E_f/E_m is shown in Fig. 8. It is compared with the prediction of SL, MSL, and FEA, as well as with predictions of other elasticity theories, namely, the Tsai-Halpin model (Halpin and Kardos, 1976, Halpin, 1984) and the Eshelby model (Eshelby, 1957, Tandon and Weng, 1986). The prediction given by the model of Taya and Arsenault, who neglected stress intensification at fiber ends, is shown in Fig. 8. Their equation (Taya and Arsenault, 1989) for the modulus is

$$\frac{E_c}{E_m} = V_m E_m + V_f E_m + V_f E_f \cdot \left[1+\left(\frac{E_m}{E_f}-1\right)\frac{\tanh(ns)}{ns}\right] \tag{28}$$

The modulus results from their model are slightly higher than those of the original shear lag model, but still substantially underestimate the actual composite modulus. Superimposed on Fig. 8 are the available experimental data for SiC whisker reinforced Al alloys. Note that the MSL predictions agree most closely with FEA results. Therefore, it is found that the shear lag approach taking end effects into account is physically most realistic. All methods, except the SL model and the Taya-Arsenault model, however, are reasonably comparable with available data. The SL model and Taya-Arsenault model is clearly an underestimation. However, as the aspect ratio is increased the predictions of all models converge to the ROM predictions as expected.

4.3 Small scale yielding predictions of composite

Figure 9 shows the normalized composite proportional limit as a function of modulus ratio and unit cell geometry in the case of a fixed whisker

volume fraction and whisker aspect ratio. As can be seen in Fig. 9, the composite proportional limit decreases as the modulus ratio increases. Stress intensification at the tip of the fiber or whisker results in small scale yielding in the composite prior to the matrix proportional limit. The small scale yielding is more enhanced for the case of smaller end gap ratio, or smaller RVE aspect ratio, in which case the stress concentrations are larger at fiber ends. Figure 9 also compares the MSL closed form predictions to numerical results from FEA. Good qualitative and quantitative agreement is obtained between the closed form and numerical predictions, at least on the smaller end gap size regions pertinent to actual composites. As discussed previously (Kim, 1994), MSL predictions become more approximate as end gap sizes become large. Note that the experimental result falls in the range of the predicted values.

5. Conclusions

An extension of modified shear lag model has been rigorously studied. The results in modulus predictions of the present model were most closely matched with FEA computations compared with those of other models. It is evident that the inaccurate predictions of the original shear lag theory for small aspect ratio are due to its neglect of the influence of fiber end regions. It was found that the MSL model which is applicable to small scale yielding predictions associated with plastic deformation at fiber or whisker ends conforms with FEA predictions. It was also found that, when the fiber modulus increased or when the end gap size is reduced, the localized plasticity in the vicinity of fiber ends is initiated before the applied stress reaches the matrix yield stress.

Acknowledgement

This work was supported by the 1996 Jeonju University research fund.

References

Agarwal, B. D., Lifsitz, J. M., and Broudtman, L. J., 1974, "Elastic-Plastic Finite Element Analysis of Short Fiber Composites," *Fiber Science and Technology*, Vol. 7, pp. 45~62.

Aresenault, R. J., 1983, "Interfaces in Metal Matrix Composites," *Scripta Metallurgica*, Vol. 18, pp. 1131~1134.

Arsenault, R. J., 1984, "The Strengthening of Aluminum Alloy 6061 by Fiber and Platelet Silicon Carbide," *Materials Science and Engineering*, Vol. 64, pp. 171~181.

Budiansky, B., 1965, "On the Elastic Modulus of Some Heterogeneous Materials," *Journal of the Mechanics and Physics of Solids*, Vol. 13, pp. 223~227.

Cook, R. D., Malkua, D. S. and Plesha, M. E., 1989, *Concepts and Applications of Finite Element Analysis*, John Wiley and Sons, Third Edition, pp. 163~295.

Cox, H. L., 1952, "The Elasticity and Strength of Paper and Other Fibrous Materials," *British Journal of Applied Physics*, Vol. 3, pp. 72~79.

Eshelby, J. D., 1957, "The Determination of the Elastic Field of an Ellipsoidal Inclusion, and Related Problems," *Proceedings of the Royal Society, London*, Vol. A241, pp. 376~396.

Halpin, J. C., 1984, *Primer on Composite Materials: Analysis*, Technomic Publishing Co., Inc., pp. 130~141.

Halpin, J. C., and Kardos, J. L., 1976, "The Halpin-Tsai Equations: A Review," *Polymer Engineering and Science*, Vol. 16, No. 5, pp. 344~352.

Hashin, Z., 1983, "Analysis of Composite Materials," *Journal of Applied Mechanics*, Vol. 50, pp. 481~505.

Hashin, Z. and Shtrikman, S., 1962, "On Some Variational Principles in Anisotropic and Nonhomogeneous Elasticity," *Journal of the Mechanics and Physics of Solids*, Vol. 10, pp. 335~332.

Hashin, Z. and Shtrikman, S., 1963, "A Variational Approach to the Theory of the Elastic Behavior of Multiphase Materials," *Journal of the Mechanics and Physics of Solids*, Vol. 11, pp. 127~140.

Hershey, A. V., 1954, "The Elasticity of an Isotropic Aggregate of an Anisotropic Cubic

Crystals," *Journal of Applied Mechanics*, Vol. 21, pp. 236~240.

Hill, R., 1965a, "Theory of Mechanical Properties of Fiber-Strengthened Materials-III, Self-Consistent Model," *Journal of the Mechanics and Physics of Solids*, Vol. 13, pp. 189~198.

Hill, R., 1965b, "A Self-Consistent Mechanics of Composite Materials," *Journal of the Mechanics and Physics*, Vol. 13, pp. 213~222.

Kim, H. G. and Nair, S. V., 1990, "Strengthening Analysis of SiC Whisker Reinforced Aluminum Alloys," *Proceedings of the 11th World Korean Scientists and Engineers Conference*, The Korean Federation of Science and Technology Societies, Seoul, Korea, June. 25-29, pp. 1737~1742.

Kim, H. G. and Chang, I., 1995, "Analysis of the Strengthening Mechanism Based on Stress-Strain Hysteresis Loop in Short Fiber Reinforced Metal Matrix Composites," *KSME International Journal*, Vol. 9, No. 2, pp. 197~208.

Kim, H. G., 1994, "Stress Transfer in Shear Deformable Discontinuous Composites," *KSME International Journal*, Vol. 8, No. 4, pp. 475~484.

Kohnke, P. C., 1989, *ANSYS Theoretical Manual, 5th Edition*, Swanson Analysis Systems Inc., Houston, PA.

Kroner, E., 1958, "Berechnung del elastischen Konstanten des Vielkristalls aus den Konstanten del Einkristalls," *Zeitschrift fur Physik*, Vol. 151, pp. 504~518.

Muki, R. and Sternberg, E., 1969, "On the Diffusion of an Axial Load fron an Infinite Cylindrical Bar Embedded in an Elastic Medium," *International Journal of Solids and Structures*, Vol. 5, pp. 587~605.

Nair, S. V., Tien, J. K. and Bates, R. C., 1985 "SiC-Reinforced Aluminum Metal Matrix Composites," *International Metals Review*, Vol. 30, No. 6, pp. 275~290.

Nair, S. V. and Kim, H. G.: "Thermal Residual Stress Effects on Constitutive Response of a Short Fiber or Whisker Reinforced Metal Matrix Composite," *Scripta Metallurgica*, Vol. 25, No. 10, pp. 2359~2364 (1991).

Nardone, V. C., 1987, "Assessment of Models Used to PRedict the Strength of Discontinuous Silicon Carbide Reinforced Aluminum Alloys," *Scripta Metallurgica*, Vol. 21, pp. 1313~1318.

Nardone, V. C. and Prewo, K. M., 1986, "On the Strength of Discontinuous Silicon Carbide Reinforced Aluminum Composites," *Scripta Metallurgica*, Vol. 20, pp. 43~48.

Nutt, S. R. and Needleman, A., 1987, "Void NUcleation at Fiber Ends in Al-SiC Composites," *Scripta Metallurgica*, Vol. 21, pp. 705~710.

Paul, B., 1960, "Prediction of Elastic Constants of Multiphase Materials," *Transaction of the Metallurgical Society of AIME*, Vol. 218, pp. 36~46.

Piggot, M. R., 1980, *Load Bearing Fiber Composites*, Pergamon Press, pp. 83~99.

Sternberg, E. and Muki, R., 1970, "Load-Absorption by a Filament in Fiber Reinforced Material," *Journal of Applied Mathematics and Physics (ZAMP)*, Vol. 21, pp. 552~569.

Tandon, G. P. and Weng, G. J., 1986, "Stress Distribution In and Around Spheroidal Inclusions and Voids at Finite Concentration," *Journal of Applied Mechanics*, Vol. 53, pp. 511~518.

Taya, M., and Arsenault, R. J., 1987, "A Comparison between a Shear Lag Type Model and an Eshelby Type Model in Predicting the Mechanical Properties of Short Fiber Composite," *Scripta Metallurgica*, Vol. 21, pp. 349~354.

Taya, M. and Aresenault, R. J., 1989, *Metal Matrix Composites: Thermomechanical Behavior*, Pergamon Press, pp. 25~28.